arXiv:2605.16755v1 [cs.LG] 16 May 2026

Learning Unbiased Permutations via Flow Matching

Yimeng Min
Department of Computer Science
Cornell University
Ithaca, NY, USA
min@cs.cornell.edu

Carla P. Gomes
Department of Computer Science
Cornell University
Ithaca, NY, USA
gomes@cs.cornell.edu

Abstract

Learning permutations is fundamental to sorting, ranking, and matching, but existing differentiable methods based on entropy-regularized Sinkhorn produce a single softened solution and collapse under ambiguity. We present PermFlow, a conditional flow matching framework that operates directly on the affine subspace of matrices with unit row and column sums. A closed-form tangent-space projector preserves these constraints exactly along every trajectory, by construction rather than through iterative correction, and a nearest-target coupling routes distinct noisy initializations toward distinct valid permutations. The result is a model that captures multimodal permutation distributions rather than collapsing them to a single mode. On a visual sorting task with blended-digit ambiguity and a symmetric linear assignment problem, PermFlow achieves high accuracy on unambiguous inputs and recovers both valid permutations under ambiguity, where Sinkhorn-based baselines structurally fail.

1 Introduction

Flow-based generative models have emerged as a powerful generative modeling paradigm, achieving widespread adoption across diverse domains such as computer vision and natural language processing. In these settings, the data lie in continuous spaces (e.g., high-dimensional vectors), where flows offer a principled mechanism for transforming simple noise into complex, structured outputs. Concretely, Flow Matching learns by regressing onto conditional velocity fields that transport individual samples; integrating this learned dynamics then yields a model capable of generating the full data distribution [Chen and Lipman, 2023, Tong et al., 2023, Esser et al., 2024, Kornilov et al., 2024, Sriram et al., 2024, Chen and Lipman, 2023].

However, this paradigm becomes significantly more challenging when we move to discrete combinatorial structures. Objects such as permutations, matchings, and tours obey strict structural constraints. For instance, a permutation matrix must contain exactly one "1" in each row and each column. As a result, these objects reside on highly constrained geometric spaces rather than in the unconstrained ambient space $\mathbb{R}^{n\times n}$, making the direct application of standard flow-based methods nontrivial.

Most existing approaches deal with this difficulty by relaxing the problem. They replace permutations with continuous approximations (for example, using entropy-regularized Sinkhorn layers) and later round the solution back to a discrete one. While this makes optimization easier, it changes the geometry of the problem and can introduce bias or inconsistencies between training and testing. In particular, these methods usually produce a single softened solution and do not naturally represent uncertainty when multiple permutations are equally valid [Sinkhorn, 1967]. This is a real limitation in many settings where the supervision is set-valued rather than single-valued: there may be many feasible (and essentially equally good) permutations consistent with the input.

Preprint.

For example, in matching or assignment problems with symmetries, repeated or indistinguishable items, or near-ties in cost, multiple permutations can explain the same observation. Yet a deterministic pipeline will still collapse everything into a single argmax permutation, committing to one choice and discarding alternative valid orderings. In contrast, what we often want is not one "best" permutation but a distribution over optimal permutations, allowing us to quantify ambiguity, sample diverse valid solutions, and propagate uncertainty downstream.

Furthermore, entropy regularization introduces a well-known bias: the entropic term favors high-entropy solutions, pushing mass toward the interior of the Birkhoff polytope and away from permutation vertices. This alters the optimization landscape relative to the original combinatorial problem and, when combined with discrete rounding at inference time, leads to a mismatch between training and inference objectives [Janati et al., 2020].

In this work, we present Affine Permutation Flow (PermFlow). Instead of relaxing the structural constraints into an unconstrained continuous space, we directly design flow dynamics that respect the geometry of permutation matrices from the outset. We use Conditional Flow Matching (CFM) to learn velocity fields directly. By projecting the learned velocities onto the correct tangent space (which enforces zero row and column sums), we ensure that the structural constraints are preserved throughout training. This allows us to train flow-based models without relying on entropy regularization or ad hoc projection steps. Our approach generates a set of permutations by sampling different initial noise states and integrating the learned flow dynamics. As mentioned above, in many tasks, the correct ordering is inherently ambiguous, and multiple permutations may be equally consistent with the input. Unlike deterministic relaxations such as Sinkhorn, which collapse predictions to a single mode, our stochastic flow model captures this ambiguity by representing a distribution over permutations and sampling multiple valid combinatorial solutions [Emami and Ranka, 2018, Mena et al., 2018].

2 Related Work

The dominant paradigm for differentiable permutation prediction relaxes permutation matrices $\mathcal{P}$ to the Birkhoff polytope $\mathcal{B}_+$ via entropy-regularized optimal transport [Sinkhorn, 1964, Cuturi, 2013], with applications to latent permutation learning [Mena et al., 2018], sorting [Grover et al., 2019], and combinatorial RL [Emami and Ranka, 2018]. The entropic term biases solutions toward the polytope interior [Janati et al., 2020], and deterministic Sinkhorn cannot represent multimodal posteriors; Gumbel-Sinkhorn [Mena et al., 2018] adds noise but empirically concentrates around a single soft solution. Geometric alternatives include stick-breaking parameterizations of $\mathcal{B}_+$ [Linderman et al., 2018] and Riemannian Langevin sampling with retraction-based integrators [Birdal and Simsekli, 2019]. We share the geometric viewpoint but work in the affine setting, which admits a closed-form orthogonal projector and removes the need for retractions, and we learn input-conditioned dynamics rather than fixed MCMC. Our construction builds on flow matching [Lipman et al., 2022] and Conditional Flow Matching [Tong et al., 2023], which have been extended to optimal-transport couplings [Kornilov et al., 2024], Riemannian manifolds [Chen and Lipman, 2023], and discrete state spaces [Campbell et al., 2024, Gat et al., 2024]. By contrast, generic manifold-ODE schemes enforce constraints only *approximately*: under a Lipschitz assumption on the vector field, the violation is bounded by a factor growing as e^{Lt} in integration time and $\mathcal{O}(h^p)$ in step size h, where L is the Lipschitz constant [Hairer et al., 1993]. This exponential amplification carries over to learned vector fields, where projection or retraction steps are needed to keep iterates close to the constraint set [Lou et al., 2020, Falorsi and Forré, 2020, Mathieu and Nickel, 2020, Chen and Lipman, 2023], so feasibility degrades with both network expressivity (which controls L) and integration horizon.

Our contributions are threefold: 1. We propose a CFM framework for learning distributions over permutations. Our method parameterizes a velocity field directly on the affine subspace defined by the row- and column-sum constraints, and projects it onto the corresponding tangent space. As a result, these constraints hold exactly at every t and for any f_θ, with no Lipschitz or smoothness assumption beyond ODE existence. This avoids entropic smoothing and explicit positivity constraints, in contrast to Sinkhorn-style relaxations whose feasibility only holds in the limit and to generic manifold-ODE schemes whose constraint violation grows as w.r.t. to time/iterations. 2. We apply the framework to ambiguous permutation prediction, where multiple orderings are equally consistent with the input. Sinkhorn and other deterministic relaxations collapse this ambiguity into a single solution. Our stochastic flow instead learns a conditional distribution over valid permutations,

allowing explicit representation and sampling of multiple combinatorial modes. 3. Empirically, our model achieves competitive performance, showing that conditional flow matching can be extended beyond continuous domains such as vision and language to structured combinatorial objects. To our knowledge, this is one of the earliest applications of flow matching to inherently discrete permutation learning.

3 Background

3.1 Sinkhorn Iteration for Soft Permutations

Given a score matrix $S \in \mathbb{R}^{n \times n}$, the goal of permutation prediction is often formulated as a linear assignment problem

$$\max_{P \in \mathcal{P}_n} \langle S, P \rangle, \tag{1}$$

where $\mathcal{P}_n$ is the set of $n \times n$ permutation matrices. Because $\mathcal{P}_n$ is discrete, a common relaxation replaces it with the Birkhoff polytope

$$\mathcal{B}_+ = \{X \in \mathbb{R}_+^{n \times n} \mid X\mathbf{1} = \mathbf{1},\ X^\top \mathbf{1} = \mathbf{1}\}, \tag{2}$$

the set of doubly stochastic matrices. To obtain a differentiable solution, entropy regularization is introduced:

$$\max_{X \in \mathcal{B}_+} \langle S, X \rangle + \tau H(X), \tag{3}$$

where $H(X)$ is the Shannon entropy and $\tau > 0$ is a temperature parameter. The solution takes the form

$$X^\star = \mathrm{Diag}(u)\, K\, \mathrm{Diag}(v), \qquad K = \exp(S/\tau), \tag{4}$$

where scaling vectors u and v enforce row and column normalization. These vectors can be computed efficiently by alternating row and column normalization [Sinkhorn, 1964]. In practice, the resulting matrix X is a soft permutation (doubly stochastic matrix). As $\tau \to 0$, the solution becomes closer to a permutation matrix but gradients become unstable. Larger values of τ produce smoother but less discrete solutions.

Although Sinkhorn provides a useful differentiable relaxation, it typically produces a *single* softened solution. When multiple permutations are equally valid, for example due to symmetries or near-ties in scores, the entropy-regularized objective selects one solution in the Birkhoff polytope and collapses the others. As a result, Sinkhorn-based methods do not naturally represent uncertainty or generate diverse valid permutations.

3.2 Flow Matching and Conditional Flow Matching

Flow Matching is a generative framework that learns a continuous transport process transforming samples from a source distribution p_0 into samples from a target distribution p_1. Given noisy samples $\mathbf{x}_0 \sim p_0$ and clean samples $\mathbf{x}_1 \sim p_1$, the goal is to learn a time-dependent velocity field $u_t(\mathbf{x}_t)$ that transports probability mass from p_0 to p_1. Let $\psi_t(\mathbf{x}_0 \mid \mathbf{x}_1)$ denote an interpolant that defines the trajectory between $\mathbf{x}_0$ and $\mathbf{x}_1$. The interpolant satisfies the boundary conditions

$$\psi_0(\mathbf{x}_0 \mid \mathbf{x}_1) = \mathbf{x}_0, \qquad \psi_1(\mathbf{x}_0 \mid \mathbf{x}_1) = \mathbf{x}_1. \tag{5}$$

At time $t \in [0, 1]$, the intermediate point is $\mathbf{x}_t = \psi_t(\mathbf{x}_0 \mid \mathbf{x}_1)$. The conditional velocity field is defined as the time derivative of the interpolant:

$$u_t(\mathbf{x}_t \mid \mathbf{x}_1) = \frac{d}{dt}\psi_t(\mathbf{x}_0 \mid \mathbf{x}_1). \tag{6}$$

For a velocity field u_t to generate the evolving distribution p_t, it must satisfy the continuity equation

$$\frac{\partial}{\partial t} p_t(\mathbf{x}) = -\nabla \cdot \big(p_t(\mathbf{x}) u_t(\mathbf{x})\big), \tag{7}$$

where $\nabla\cdot$ denotes the divergence operator. Flow matching objective trains a parameterized velocity model $u_\theta(\mathbf{x}_t, t)$ to approximate the true marginal velocity field:

$$\mathcal{L}_{\text{FM}} = \mathbb{E}_{t, \mathbf{x}_t}\left[\|u_\theta(\mathbf{x}_t, t) - u_t(\mathbf{x}_t)\|^2\right]. \tag{8}$$

However, computing the marginal velocity $u_t(\mathbf{x}_t)$ requires integrating over all trajectories connecting p_0 and p_1, which is generally intractable. To address this issue, CFM conditions the velocity field on individual data samples $\mathbf{x}_1$. The resulting CFM objective becomes

$$\mathcal{L}_{\text{CFM}} = \mathbb{E}_{t,\mathbf{x}_0,\mathbf{x}_1}\left[\|u_\theta(\mathbf{x}_t, t) - u_t(\mathbf{x}_t \mid \mathbf{x}_1)\|^2\right]. \tag{9}$$

Importantly, the conditional and unconditional objectives share the same gradient:

$$\mathcal{L}_{\text{FM}} = \nabla_\theta \mathcal{L}_{\text{CFM}}, \tag{10}$$

making the conditional formulation both tractable and theoretically consistent [Lipman et al., 2022].

4 Geometry-Preserving Permutation Flow

Before describing the construction, we highlight the kind of guarantee we aim for. Existing approaches keep iterates feasible only *approximately*: Sinkhorn alternates row and column normalization and leaves a residual that shrinks with iteration count, while generic manifold-ODE schemes bound the constraint violation only up to a factor that grows as e^{Lt} under a Lipschitz assumption on the vector field, with L denotes the Lipschitz constant. In both cases, feasibility degrades with network expressivity or integration time. We aim for a stronger property. We work on the affine subspace of matrices with row and column sums equal to one, and build a projector $\mathcal{C}$ such that $\mathcal{C}(U)$ lies in the corresponding tangent space for *every* matrix U, as an algebraic identity. Substituted into the flow, the row- and column-sum constraints hold *exactly* at every t, for any f_θ, with no Lipschitz or smoothness assumption beyond ODE existence. Figure 1 compares this guarantee against existing strategies.

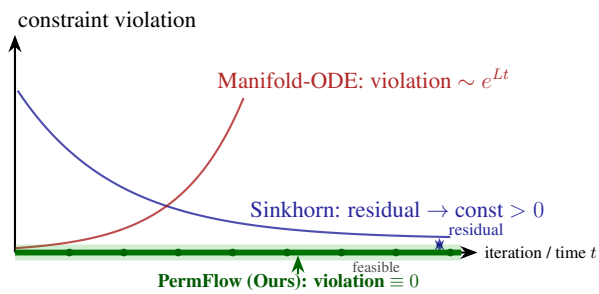

Figure 1: Feasibility behavior of different methods. Sinkhorn leaves a non-vanishing residual; manifold-ODE schemes incur exponentially growing violation $\sim e^{Lt}$. **PermFlow (ours)** maintains exact feasibility at every step.

We model permutations through continuous dynamics on the affine constraint manifold. Let $\mathbf{1} \in \mathbb{R}^n$ denote the all-ones vector, and endow $\mathbb{R}^{n\times n}$ with the Frobenius inner product $\langle A, B\rangle_F = \operatorname{tr}(A^\top B)$. The affine constraint manifold is the set of matrices whose rows and columns each sum to one,

$$\mathcal{B}_a \;=\; \{X \in \mathbb{R}^{n\times n} : X\mathbf{1} = \mathbf{1},\; X^\top\mathbf{1} = \mathbf{1}\}, \tag{11}$$

and at any point of $\mathcal{B}_a$ the admissible directions of motion are those that preserve these row and column sums:

$$T \;=\; \{\Delta \in \mathbb{R}^{n\times n} : \Delta\mathbf{1} = 0,\; \Delta^\top\mathbf{1} = 0\}. \tag{12}$$

Note that T does not depend on the base point, since $\mathcal{B}_a$ is affine.

To map arbitrary matrices onto T, we use the centering operator $\mathcal{C} : \mathbb{R}^{n\times n} \to \mathbb{R}^{n\times n}$,

$$\mathcal{C}(U) \;=\; U \;-\; \tfrac{1}{n}U\mathbf{1}\mathbf{1}^\top \;-\; \tfrac{1}{n}\mathbf{1}\mathbf{1}^\top U \;+\; \tfrac{1}{n^2}\mathbf{1}\mathbf{1}^\top U\mathbf{1}\mathbf{1}^\top. \tag{13}$$

The first correction term subtracts each row's mean, the second subtracts each column's mean, and the third adds back the global mean to avoid double-counting. A direct calculation confirms that $\mathcal{C}(U)\mathbf{1} = 0$ and $\mathbf{1}^\top\mathcal{C}(U) = 0$, so $\mathcal{C}(U)$ always lies in T.

Theorem 1 (Geometric correctness of PermFlow)**.** *The centering operator $\mathcal{C}$ is the orthogonal projector onto T. Consequently, the ODE*

$$\dot{X}_t \;=\; \mathcal{C}\big(f_\theta(X_t, t)\big), \qquad X_0 \in \mathcal{B}_a, \tag{14}$$

satisfies $X_t \in \mathcal{B}_a$ for all $t \geq 0$, for any choice of f_θ.

Algorithm 1 PermFlow for Permutation Distribution Learning

Require: Input context $\mathbf{c}$; valid target permutations $\{P^1, \ldots, P^M\} \subset \{0,1\}^{n\times n}$ (set $M = 1$ for unambiguous inputs); encoder g_ϕ; velocity network f_θ; noise scale σ_0; ODE steps S; samples K, input context $\mathbf{c}$.

Tangent projector. $\mathcal{C}(U) \leftarrow U - \frac{1}{n}U\mathbf{1}\mathbf{1}^\top - \frac{1}{n}\mathbf{1}\mathbf{1}^\top U + \frac{1}{n^2}\mathbf{1}\mathbf{1}^\top U\mathbf{1}\mathbf{1}^\top$

Training.

for each minibatch $(\mathbf{c},\ P^1, \ldots, P^M)$ **do**

  $\mathbf{h} \leftarrow g_\phi(\mathbf{c})$ ▷ encode context once per batch

  $\varepsilon \sim \mathcal{N}(0, I);\quad \tilde{X}_0 \leftarrow \mathcal{C}\big(\frac{1}{n}\mathbf{1}\mathbf{1}^\top + \sigma_0\,\varepsilon\big)$ ▷ project perturbed matrix onto tangent space

  $P^* \leftarrow \arg\min_{P^m} \|\tilde{X}_0 - P^m\|_F$ ▷ coupling: nearest valid target wins

  $t \sim \mathrm{Unif}(0,1);\quad X_t \leftarrow (1-t)\,\tilde{X}_0 + t\,P^*$ ▷ interpolated path point

  $\varepsilon' \sim \mathcal{N}(0, I);\quad \hat{X}_t \leftarrow \mathcal{C}(X_t + \sigma_t\,\varepsilon')$ ▷ perturb interpolant and re-project

  $\dot{X} \leftarrow P^* - \tilde{X}_0$ ▷ constant target velocity

  $\mathcal{L} \leftarrow \|v_\theta(\hat{X}_t, \mathbf{h}) - \dot{X}\|_F^2;\quad$ update (ϕ, θ) via $\nabla\mathcal{L}$ ▷ CFM regression loss

end for

Inference *(K trajectories, S Euler steps each).*

$\mathbf{h} \leftarrow g_\phi(\mathbf{c})$ ▷ encode once, shared across all K trajectories

for $k = 1, \ldots, K$ **do**

  $\varepsilon^{(k)} \sim \mathcal{N}(0, I);\quad X^{(k)} \leftarrow \mathcal{C}\big(\frac{1}{n}\mathbf{1}\mathbf{1}^\top + \sigma_0\,\varepsilon^{(k)}\big)$ ▷ fresh noise ⇒ diverse trajectory starts

  for $s = 0, \ldots, S-1$ **do**

    $X^{(k)} \leftarrow X^{(k)} + \frac{1}{S}\cdot v_\theta(X^{(k)}, \mathbf{h})$ ▷ Euler step

  end for

  $\hat{P}^{(k)} \leftarrow \mathrm{Round}(X^{(k)})$ ▷ Hungarian rounding to nearest permutation

end for

return $\{\hat{P}^{(k)}\}_{k=1}^K$ ▷ diverse samples covering valid permutation modes

A full proof is given in Appendix A. Three features make the argument particularly clean. First, the four-term formula for $\mathcal{C}$ can be rewritten as a single sandwich, $\mathcal{C}(U) = (I-J)\,U\,(I-J)$, where $J = \frac{1}{n}\mathbf{1}\mathbf{1}^\top$ is the rank-one matrix that averages a vector. Since $I - J$ is itself an orthogonal projector, every property we need follows from the single identity $(I-J)^2 = I - J$: idempotency, self-adjointness, and the fact that $\mathcal{C}$ maps onto exactly T. Second, the construction is not specific to permutation matrices. Any affine subspace of $\mathbb{R}^{n\times n}$ defined by linear row or column constraints admits an analogous projector built the same way, so the trick is an instance of a general geometric principle. Third, the flow-invariance claim requires no Grönwall inequality, no Lipschitz assumption on f_θ, and no smoothness beyond what is needed for the ODE to exist. The constraint is preserved as an exact algebraic identity along trajectories, not as a small-error bound that grows with time. This is why PermFlow can claim that the row and column sums are preserved *exactly* rather than approximately, a strictly stronger guarantee than entropy-regularized relaxations can offer.

Putting the pieces together, we parameterize a velocity field with a neural network $f_\theta(X, t) \in \mathbb{R}^{n\times n}$ and project its output onto the tangent space before using it,

$$v_\theta(X, t) \;=\; \mathcal{C}\big(f_\theta(X, t)\big). \tag{15}$$

The permutation dynamics are then given by the neural ODE

$$\frac{dX_t}{dt} \;=\; v_\theta(X_t, t), \qquad X_0 \in \mathcal{B}_a. \tag{16}$$

Because the velocity always lies in T, the row and column sums of X_t do not change along a trajectory, so X_t stays on $\mathcal{B}_a$ for all t no matter what the network outputs.

As shown in Figure 4, our model learns a generative flow directly in the space of permutation matrices. We start from a uniform doubly stochastic matrix $X_0 = \frac{1}{n}\mathbf{1}\mathbf{1}^\top$ and add Gaussian noise to obtain a perturbed initialization $\tilde{X}_0 = X_0 + \sigma_0\varepsilon$, where σ_0 is noise scale and $\varepsilon \sim \mathcal{N}(0, I)$. To preserve the structural constraints of permutation matrices, the noise is projected onto the tangent space using $\mathcal{C}(U)$, which enforces zero row and column sums. Given a noisy matrix $\tilde{X}_0$, we define a coupling with valid permutation targets using a *nearest-valid-target-wins* rule. Among the set of

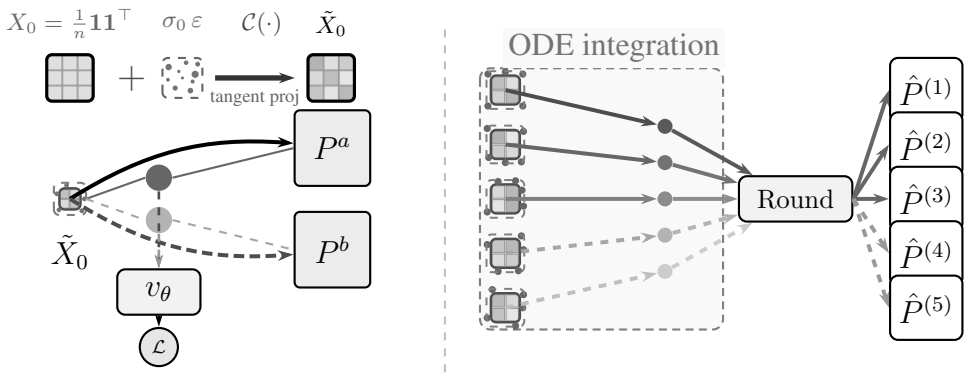

Figure 2: Our model: noise is added to the uniform X_0 and projected to the tangent space. Training learns a velocity field via conditional flow matching to the nearest valid permutation, while inference integrates the ODE and rounds to obtain candidate permutations.

valid permutations $\{P^1, \ldots, P^M\}$, the target permutation $P^\star$ is selected as

$$P^\star = \underset{P \in \{P^1,\ldots,P^M\}}{\arg\min} \|\tilde{X}_0 - P\|_F. \tag{17}$$

This coupling defines the endpoint of the transport path used during training. We then sample interpolation points

$$X_t = (1-t)\tilde{X}_0 + tP^\star, \quad t \sim \mathcal{U}(0,1), \tag{18}$$

and train a neural velocity field $v_\theta(X_t, t)$ using conditional flow matching to predict the transport dynamics that move samples toward the target permutation distribution. The objective minimizes the discrepancy between the predicted velocity and the analytically defined conditional velocity along this path:

$$\mathcal{L}_{\text{CFM}} = \mathbb{E}_{t,\tilde{X}_0,P^\star}\left[\left\|v_\theta(X_t, h) - \dot{X}\right\|_F^2\right], \tag{19}$$

where $h = g_\phi(c)$ is the context encoding and $\dot{X} = P^\star - \tilde{X}_0$ is the analytically defined constant conditional velocity along the linear interpolation path. The nearest-target coupling plays a central role: by anchoring each noisy initialization to its closest valid permutation, it ensures that trajectories originating from different regions of the $\mathcal{B}_a$ are directed toward distinct permutations. This prevents gradient cancellation, which would otherwise occur when conflicting targets impose opposing velocity directions on nearby points and encourages the learned flow to develop bifurcating dynamics. As a result, the model captures the full multimodal structure of the target distribution, assigning distinct trajectory branches to each valid permutation mode rather than collapsing to a single averaged solution.

At inference, K independent noisy initializations: $\tilde{X}_0^{(k)} = \mathcal{C}\big(\frac{1}{n}\mathbf{1}\mathbf{1}^\top + \sigma_0\varepsilon^{(k)}\big)$, $\varepsilon^{(k)} \sim \mathcal{N}(0, I)$, are drawn and projected onto the tangent space using $\mathcal{C}$. Each is evolved independently through the learned ODE dynamics via S Euler steps: $X^{(k)} \leftarrow X^{(k)} + \frac{1}{S} \cdot v_\theta\big(X^{(k)}, h\big)$. Because each trajectory starts from a distinct noise seed, the learned velocity field routes them toward different modes of the permutation distribution, producing diverse continuous endpoints on the affine constraint manifold. Each endpoint is then mapped to a discrete permutation via Hungarian rounding:

$$\hat{P}^{(k)} = \text{Round}\Big(X^{(k)}\Big), \tag{20}$$

yielding a set of candidate permutations $\{\hat{P}^{(k)}\}_{k=1}^K$ that collectively cover the valid modes of the target distribution.

Difference from Entropy-regularized Sinkhorn Sinkhorn methods approximate permutations via entropy regularization and repeated row/column normalization. We instead learn a flow whose velocities are projected onto the $\mathcal{B}_a$, preserving the constraint at every step. We further show in Appendix F that PermFlow is unbiased in the population limit.

5 Experiment Settings

We evaluate our method on two tasks: a visual sorting problem with ambiguity, and a symmetric assignment problem with structural ambiguity. Together they test whether the model is both accurate on unambiguous inputs and able to represent multiple valid permutations when they exist.

5.1 Permutation Learning from Visual Sequences

We evaluate on a sequence sorting task built on MNIST. Each input is a sequence of $N = 9$ digit images in an arbitrary order; the model must produce a distribution over permutation matrices that sort them by ascending digit value. *Ambiguous* sequences contain one blended image $\mathbf{x}_{\text{blend}} = \alpha\,\mathbf{x}_a + (1-\alpha)\,\mathbf{x}_b$ with $\alpha \sim \text{Beta}(2, 2)$ clipped to $[0.2, 0.8]$, admitting two valid sorted orders P_a^* and P_b^*, as shown in Figure 3. Dataset construction and training details are given in Appendix B.

Table 1: Full NoisyMNIST evaluation across K ($N = 9$, 2,000 ambiguous test sequences). Gumbel-Sinkhorn results are shown at $\tau = 0.2$ (best by clean accuracy + coverage@10; all temperatures give $\approx 0\%$ on accuracy metrics). Clean accuracy uses a single sample. † GS calibration ≈ 0.504 is degenerate (neither mode found, $\hat{f}_a = 0$, error $\approx \alpha$).

Method	K	Clean acc.	Coverage@K	Any-correct@K	Cal. error
Gumbel-Sinkhorn	5	0.3%	0.0%	0.5%	$0.504^\dagger$
	10	0.3%	0.0%	0.4%	$0.504^\dagger$
	20	0.3%	0.0%	1.1%	$0.504^\dagger$
	50	0.3%	0.0%	2.9%	$0.504^\dagger$
PermFlow	5	98.0%	91.3%	98.9%	0.244
	10	97.9%	98.2%	99.2%	0.214
	20	97.9%	99.0%	99.4%	0.196
	40	98.0%	99.2%	99.5%	0.184
	60	98.0%	99.2%	99.4%	0.183
	80	98.0%	99.2%	99.5%	0.181
	100	98.1%	99.2%	99.6%	0.181

Clean sequences have a unique ground-truth permutation, so we draw K samples and report *exact-match accuracy*. Ambiguous sequences admit two valid permutations P_a^* and P_b^* with blend weight α, and we draw K samples per instance to measure three properties: *Coverage@K*, the fraction of instances for which both P_a^* and P_b^* appear among the K samples (mode representation); *Any-correct@K*, the fraction for which at least one sample matches either valid permutation (oracle accuracy); and *calibration error* $|\hat{f}_a - \alpha|$, the absolute gap between the empirical fraction $\hat{f}_a$ of samples matching P_a^* and the true blend weight (0 = perfectly calibrated). Throughout, a prediction $\hat{P}$ counts as matching a target P^* only if $\hat{P} = P^*$ exactly after rounding.

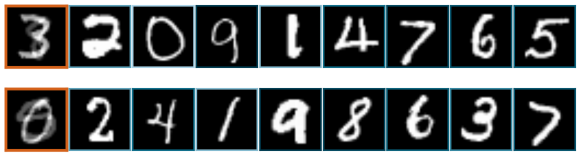

Figure 3: Illustration of the digit sorting task. Each input is a sequence of nine MNIST digits in arbitrary order, and the model must produce a permutation that sorts them in ascending order. The highlighted (orange) image in each row is a blended digit, which admits two valid sorted orderings P_a^* and P_b^* depending on which digit it is identified with.

Figure 4 shows training dynamics over 300 epochs. The CFM loss drops sharply in the first ten epochs (0.056 $\rightarrow$ 0.015) and plateaus at 0.014. Clean accuracy reaches 96.7% by epoch 10 and saturates at $\approx 98\%$. Mode coverage@10 rises to 94.3% by epoch 10 and stabilises at 97–99% thereafter, confirming the velocity field learns a bifurcating structure early and maintains it. Calibration error falls from 0.30 at epoch 1 to 0.22 by epoch 10 and remains stable at ≈ 0.21 for the remainder of training, indicating a persistent but bounded miscalibration between sampling frequency and the true blend weight α.

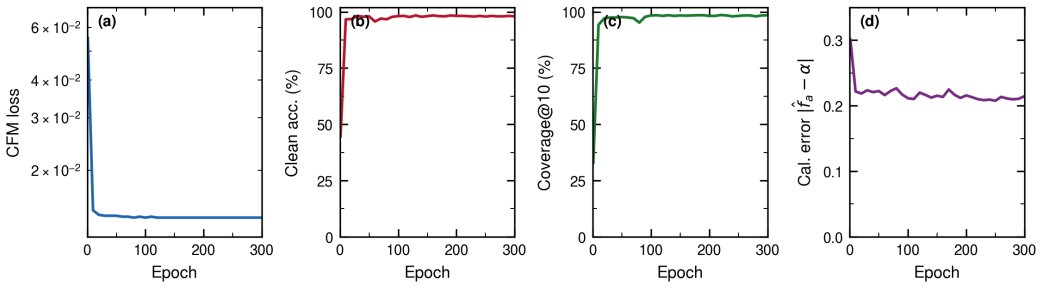

Figure 4: NoisyMNIST training dynamics. *(a):* CFM loss. *(b):* clean accuracy. *(c):* mode coverage@10. *(d):* calibration error $|\hat{f}_a - \alpha|$. All metrics stabilize within the first 10 epochs.

Table 1 compares our model with Gumbel-Sinkhorn. Gumbel-Sinkhorn achieves 0% coverage and $\approx$0% clean accuracy at every temperature ($\tau \in \{0.05, \ldots, 5.0\}$), with a degenerate calibration error of ≈ 0.504. The failure is structural: the score matrix produced by the velocity network is a flow direction calibrated to the CFM objective, not an assignment probability; Gumbel perturbations on this score yield near-uniform doubly-stochastic matrices that round to arbitrary permutations. A detailed analysis is given in Appendix C.

5.2 Distribution Learning over Optimal Assignments

The linear assignment problem asks: given n agents and n tasks with a cost $C[i, j]$ for pairing agent i with task j, find the one-to-one matching that minimises the total cost $\sum_i C[i, P[i]]$. We study the *symmetric* variant (SLAP), where $C = C^\top$. Symmetry makes the problem structurally degenerate: any optimal matching P coexists with equally cheap alternatives that arise from swapping matched pairs. We focus on *bimodal* instances, which have exactly two globally optimal matchings P_a and P_b that differ by swapping a single pair of assignments. The Hungarian algorithm finds *one* optimum in polynomial time; our goal is harder, to learn a distribution that samples *both* P_a and P_b with equal frequency and never misses either. Dataset construction is detailed in Appendix D.

Table 2: SLAP results across K at $N = 20$ and $N = 100$ (2,000 bimodal test instances each). GS shown at $\tau = 0.5$; all temperatures give 0%. Clean accuracy and optimality gap use a single sample. † GS balance $= 0$ is degenerate (no mode found); PermFlow's 0.0000 at $N = 100$ is genuine (both modes sampled equally).

Method	N	K	Clean acc.	Coverage@K	Any-correct@K	Opt. gap Δ	Balance
Gumbel-Sinkhorn	20	any	0.0%	0.0%	0.0%	0.52	0.000†
Gumbel-Sinkhorn	100	any	0.0%	0.0%	0.0%	0.85	0.000†
		5	94.5%	94.0%	94.3%	0.0217	0.0015
		10	94.5%	94.5%	95.0%	0.0216	0.0014
		20	94.2%	95.0%	95.4%	0.0217	0.0013
PermFlow	20	40	94.2%	95.3%	95.9%	0.0215	0.0012
		60	94.6%	95.5%	96.0%	0.0217	0.0012
		80	94.2%	95.5%	96.0%	0.0217	0.0009
		100	94.3%	95.7%	96.2%	0.0217	0.0012
		5	81.8%	83.0%	83.0%	0.0254	0.0000
		10	81.8%	83.9%	83.9%	0.0254	0.0000
		20	82.2%	85.2%	85.2%	0.0254	0.0000
PermFlow	100	40	82.8%	85.5%	85.5%	0.0255	0.0000
		60	81.9%	85.8%	85.8%	0.0254	0.0000
		80	81.8%	86.5%	86.5%	0.0255	0.0000
		100	81.9%	86.1%	86.1%	0.0255	0.0000

We evaluate clean instances with exact-match accuracy on a single sample. For bimodal instances we draw K samples per instance and report: *coverage@K*, the fraction for which both P_a^* and P_b^*

appear among the K samples; *any-correct@K*, the fraction for which at least one sample matches either target; *optimality gap* $\Delta = (\mathrm{cost}(\hat{P}) - \mathrm{cost}(P^*))/|\mathrm{cost}(P^*)|$, the fractional cost excess of the first sample over the Hungarian optimum; and *mode balance* $|\mathrm{freq}(P_a^*) - \mathrm{freq}(P_b^*)|$, the absolute difference between the fractions of samples matching each mode (0 = balanced, 1 = collapse).

Figure 5 shows training dynamics at $N = 20$. The CFM loss approaches zero by epoch 200, while clean accuracy and coverage@10 stabilise at 94–95% by epoch 30, indicating that the velocity field learns to cover both modes early and consistently. The optimality gap plateaus at $\approx$2.2% and mode balance stays below 0.002 throughout, confirming that the model assigns nearly equal probability to P_a and P_b. PermFlow thus learns a velocity field biased toward the specific modes in the training distribution, and X_t-conditioning further causes trajectories starting near P_a and P_b to diverge, reaching each mode independently. Clean accuracy remains stable at $\approx$94% across sampling budgets, while coverage grows only modestly with K (from 94.0% at K=5 to 95.7% at K=100), showing that most of the coverage budget is saturated after just five trajectories.

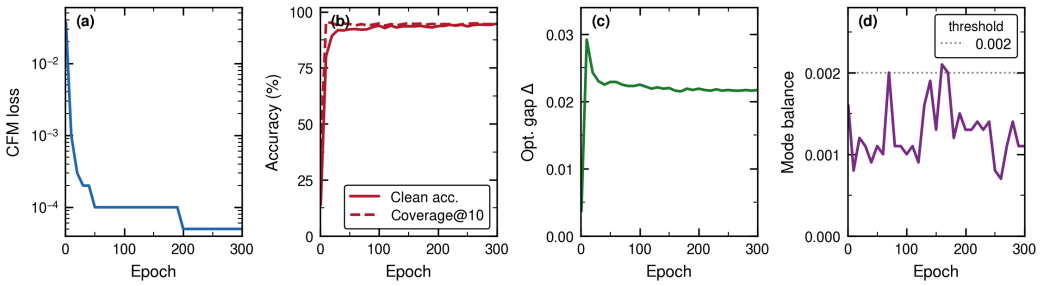

Figure 5: SLAP training dynamics. *Left:* CFM loss. *Second:* clean accuracy (solid) and coverage@10 (dashed). *Third:* optimality gap. *Right:* mode balance error (below 0.002 throughout).

Table 2 compares PermFlow with Gumbel-Sinkhorn at two problem sizes, $N = 20$ and $N = 100$. Gumbel-Sinkhorn scores 0% on every metric at every temperature in the sweep $\tau \in \{0.05, \ldots, 5.0\}$, with an optimality gap of about 0.52 at $N = 20$ and 0.85 at $N = 100$. This is a structural failure, not a tuning issue. Because $C = C^\top$, every target P_a has an inverse P_a^{-1} with identical cost, so the score $-C$ cannot distinguish the labeled matching from its symmetric counterpart. Gumbel-Sinkhorn does not see the training labels and cannot resolve this ambiguity on its own. A full proof and per-temperature breakdown are given in Appendix E. PermFlow stays accurate as the problem size grows. At $N = 20$ it reaches 94.5% clean accuracy and 94.0–95.7% coverage as K ranges from 5 to 100. At $N = 100$ it reaches 81.8% clean accuracy and 83.0–86.5% coverage on the same range. The optimality gap is small in both cases (about 0.022 at $N = 20$ and 0.025 at $N = 100$). Mode balance is essentially zero at $N = 100$, so when PermFlow recovers the optimal modes it samples both with near-equal frequency, Figure 6 in appendix shows the training dynamics of $N = 100$.

6 Conclusion

We presented PermFlow, a flow matching framework that learns distributions over permutations by flowing directly on the affine subspace of matrices with unit row and column sums. A closed-form tangent-space projector preserves feasibility exactly along every trajectory, and a nearest-target coupling routes distinct initializations toward distinct valid permutations, preventing the gradient cancellation that causes relaxation-based methods to collapse. Empirically, PermFlow recovers multiple valid permutations under ambiguity on both visual sorting and symmetric assignment, where Sinkhorn-based baselines fail structurally rather than from poor tuning. The results suggest geometry-aware flow matching as a viable alternative to entropic relaxation for combinatorial prediction problems where multiple valid solutions coexist.

References

Tolga Birdal and Umut Simsekli. Probabilistic permutation synchronization using the riemannian structure of the birkhoff polytope. In *Proceedings of the IEEE/CVF Conference on Computer Vision and Pattern Recognition*, pages 11105–11116, 2019.

Andrew Campbell, Jason Yim, Regina Barzilay, Tom Rainforth, and Tommi Jaakkola. Generative flows on discrete state-spaces: Enabling multimodal flows with applications to protein co-design. *arXiv preprint arXiv:2402.04997*, 2024.

Ricky TQ Chen and Yaron Lipman. Flow matching on general geometries. *arXiv preprint arXiv:2302.03660*, 2023.

Marco Cuturi. Sinkhorn distances: Lightspeed computation of optimal transport. *Advances in neural information processing systems*, 26, 2013.

Patrick Emami and Sanjay Ranka. Learning permutations with sinkhorn policy gradient. *arXiv preprint arXiv:1805.07010*, 2018.

Patrick Esser, Sumith Kulal, Andreas Blattmann, Rahim Entezari, Jonas Müller, Harry Saini, Yam Levi, Dominik Lorenz, Axel Sauer, Frederic Boesel, et al. Scaling rectified flow transformers for high-resolution image synthesis. In *Forty-first international conference on machine learning*, 2024.

Luca Falorsi and Patrick Forré. Neural ordinary differential equations on manifolds. *arXiv preprint arXiv:2006.06663*, 2020.

Itai Gat, Tal Remez, Neta Shaul, Felix Kreuk, Ricky TQ Chen, Gabriel Synnaeve, Yossi Adi, and Yaron Lipman. Discrete flow matching. *Advances in Neural Information Processing Systems*, 37: 133345–133385, 2024.

Aditya Grover, Eric Wang, Aaron Zweig, and Stefano Ermon. Stochastic optimization of sorting networks via continuous relaxations. *arXiv preprint arXiv:1903.08850*, 2019.

Ernst Hairer, Gerhard Wanner, and Syvert P Nørsett. *Solving ordinary differential equations I: Nonstiff problems*. Springer, 1993.

Hicham Janati, Marco Cuturi, and Alexandre Gramfort. Debiased sinkhorn barycenters. In *International Conference on Machine Learning*, pages 4692–4701. PMLR, 2020.

Nikita Kornilov, Petr Mokrov, Alexander Gasnikov, and Aleksandr Korotin. Optimal flow matching: Learning straight trajectories in just one step. *Advances in Neural Information Processing Systems*, 37:104180–104204, 2024.

Scott Linderman, Gonzalo Mena, Hal Cooper, Liam Paninski, and John Cunningham. Reparameterizing the birkhoff polytope for variational permutation inference. In *International Conference on Artificial Intelligence and Statistics*, pages 1618–1627. PMLR, 2018.

Yaron Lipman, Ricky TQ Chen, Heli Ben-Hamu, Maximilian Nickel, and Matt Le. Flow matching for generative modeling. *arXiv preprint arXiv:2210.02747*, 2022.

Aaron Lou, Derek Lim, Isay Katsman, Leo Huang, Qingxuan Jiang, Ser Nam Lim, and Christopher M De Sa. Neural manifold ordinary differential equations. *Advances in Neural Information Processing Systems*, 33:17548–17558, 2020.

Emile Mathieu and Maximilian Nickel. Riemannian continuous normalizing flows. *Advances in neural information processing systems*, 33:2503–2515, 2020.

Gonzalo Mena, David Belanger, Scott Linderman, and Jasper Snoek. Learning latent permutations with gumbel-sinkhorn networks. *arXiv preprint arXiv:1802.08665*, 2018.

Richard Sinkhorn. A relationship between arbitrary positive matrices and doubly stochastic matrices. *The annals of mathematical statistics*, 35(2):876–879, 1964.

Richard Sinkhorn. Diagonal equivalence to matrices with prescribed row and column sums. *The American Mathematical Monthly*, 74(4):402–405, 1967.

Anuroop Sriram, Benjamin K Miller, Ricky T Chen, and Brandon M Wood. Flowllm: Flow matching for material generation with large language models as base distributions. *Advances in Neural Information Processing Systems*, 37:46025–46046, 2024.

Alexander Tong, Kilian Fatras, Nikolay Malkin, Guillaume Huguet, Yanlei Zhang, Jarrid Rector-Brooks, Guy Wolf, and Yoshua Bengio. Improving and generalizing flow-based generative models with minibatch optimal transport. *arXiv preprint arXiv:2302.00482*, 2023.

A Proof of Theorem 1

The proof rests on a single algebraic identity. Let

$$J \;=\; \tfrac{1}{n}\mathbf{1}\mathbf{1}^\top$$

be the rank-one averaging matrix. Note that J is symmetric, $J^2 = J$ (so J is itself an orthogonal projector on $\mathbb{R}^n$), and $I - J$ is its orthogonal complement projector.

Lemma 2 (Sandwich identity)**.** *For all $U \in \mathbb{R}^{n\times n}$,*

$$\mathcal{C}(U) \;=\; (I-J)\,U\,(I-J).$$

Proof. Direct expansion:

$$(I-J)\,U\,(I-J) \;=\; U - JU - UJ + JUJ.$$

Substituting $J = \frac{1}{n}\mathbf{1}\mathbf{1}^\top$ gives

$$JU = \tfrac{1}{n}\mathbf{1}\mathbf{1}^\top U, \qquad UJ = \tfrac{1}{n}U\mathbf{1}\mathbf{1}^\top, \qquad JUJ = \tfrac{1}{n^2}\mathbf{1}\mathbf{1}^\top U\mathbf{1}\mathbf{1}^\top,$$

which recovers $\mathcal{C}(U)$ exactly. □

With Lemma 2 in hand, the proof of Theorem 1 proceeds in three short steps.

Step 1: $\mathcal{C}$ is idempotent ($\mathcal{C}^2 = \mathcal{C}$). Since $(I-J)^2 = I - 2J + J^2 = I - J$,

$$\mathcal{C}^2(U) \;=\; (I-J)\big[(I-J)\,U\,(I-J)\big](I-J) \;=\; (I-J)^2\,U\,(I-J)^2 \;=\; (I-J)\,U\,(I-J) \;=\; \mathcal{C}(U).$$

Step 2: $\mathrm{Im}(\mathcal{C}) = T$ and $\mathcal{C}|_T = \mathrm{id}$. For any $U \in \mathbb{R}^{n\times n}$, using $\mathbf{1}^\top(I-J) = 0$ and $(I-J)\mathbf{1} = 0$:

$$\mathcal{C}(U)\,\mathbf{1} \;=\; (I-J)\,U\,(I-J)\mathbf{1} \;=\; 0, \qquad \mathbf{1}^\top\mathcal{C}(U) \;=\; \mathbf{1}^\top(I-J)\,U\,(I-J) \;=\; 0.$$

Hence $\mathrm{Im}(\mathcal{C}) \subseteq T$. Conversely, if $\Delta \in T$, then $\Delta\mathbf{1} = 0$ implies $\Delta J = 0$, and $\mathbf{1}^\top\Delta = 0$ implies $J\Delta = 0$. So

$$\mathcal{C}(\Delta) \;=\; (I-J)\,\Delta\,(I-J) \;=\; \Delta - J\Delta - \Delta J + J\Delta J \;=\; \Delta.$$

Therefore $T \subseteq \mathrm{Im}(\mathcal{C})$ and $\mathcal{C}$ acts as the identity on T.

Step 3: $\mathcal{C}$ is self-adjoint. For any $A, B \in \mathbb{R}^{n\times n}$, using the cyclic property of the trace together with $(I-J)^\top = I - J$:

$$\langle \mathcal{C}(A), B\rangle_F = \mathrm{tr}\big((I-J)\,A\,(I-J)\,B^\top\big) = \mathrm{tr}\big(A\,(I-J)\,B^\top\,(I-J)\big) = \langle A, \mathcal{C}(B)\rangle_F.$$

Conclusion of the projector claim. A linear map that is idempotent (Step 1) and self-adjoint (Step 3) is, by definition, an orthogonal projector. Combined with the image characterization (Step 2), this proves that $\mathcal{C}$ is *the* orthogonal projector onto T.

Flow invariance. Define $\phi(t) := X_t\mathbf{1} - \mathbf{1}$. Then

$$\frac{d}{dt}\phi(t) \;=\; \dot{X}_t\,\mathbf{1} \;=\; \mathcal{C}\big(f_\theta(X_t, t)\big)\,\mathbf{1} \;=\; 0$$

by Step 2. Since $\phi(0) = X_0\mathbf{1} - \mathbf{1} = 0$, we conclude $X_t\mathbf{1} = \mathbf{1}$ for all $t \geq 0$. An identical argument applied to $\psi(t) := X_t^\top\mathbf{1} - \mathbf{1}$ gives $X_t^\top\mathbf{1} = \mathbf{1}$. Hence $X_t \in \mathcal{B}_a$ for every $t \geq 0$.

B NoisyMNIST: Experimental Details

B.1 Dataset Construction

Sequences of $N = 9$ digit images are sampled from the standard MNIST dataset. Each sequence is either *clean* or *ambiguous*.

Clean sequences. Nine digit images are drawn without replacement from MNIST and arranged in a random order. The unique ground-truth permutation sorts them by ascending digit value. Validation sequences use MNIST training images; test sequences use exclusively MNIST test images.

Ambiguous sequences. One position in the sequence holds a blended image

$$\mathbf{x}_{\text{blend}} = \alpha\, \mathbf{x}_a + (1-\alpha)\, \mathbf{x}_b, \qquad \alpha \sim \text{Beta}(2,2) \text{ clipped to } [0.2, 0.8].$$

Blend pairs (d_a, d_b) are drawn from a fixed set of eight pairs whose digit values differ by at least three: $\{(0,4),(1,5),(2,6),(3,7),(1,6),(2,7),(0,5),(3,8)\}$. This guarantees that d_a and d_b occupy genuinely different sorted positions, giving exactly two valid orderings P_a^* and P_b^*. The blend weight α is stored with each instance and used to compute calibration error at evaluation time.

Dataset splits. The training set contains 100,000 sequences with a 50% ambiguous target. Separate test sets of 2,000 clean and 2,000 ambiguous sequences are held out; all test images are drawn from the MNIST test split.

B.2 Model and Optimisation

Architecture. Each digit image is encoded independently by a small CNN: two convolutional blocks (16 and 32 filters, 3×3 kernels, BatchNorm, ReLU, MaxPool 2×2) followed by a third block (64 filters) with adaptive average pooling, projecting to $d_{\text{enc}} = 64$ via a linear layer and LayerNorm.

The N per-digit embeddings are projected to $d_{\text{model}} = 128$, augmented with learnable slot-position embeddings, and processed by a 4-layer Transformer (4 heads, FFN multiplier 4, dropout 0.1, GELU, pre-norm). A bilinear head produces the score matrix $S[i,j] = \langle h_i, r_j \rangle / \sqrt{d}$, where h_i is the contextual embedding of slot i and r_j is a learnable rank embedding; S is tangent-projected to give the velocity $v \in \mathbb{R}^{N \times N}$.

At inference, K independent trajectories each start from a distinct noisy uniform matrix

$$X_0 = T\big(\tfrac{1}{N}\mathbf{1}\mathbf{1}^\top + \sigma_0\, \varepsilon\big), \qquad \sigma_0 = 1.0,$$

where $T(\cdot)$ is the tangent-space projection and ε is a doubly-centred unit-Frobenius noise matrix. The velocity v is fixed (does not depend on X_t), so different starting points X_0 trace different trajectories and round to different permutations via the Hungarian algorithm after 10 Euler steps.

Training. AdamW ($\text{lr} = 3 \times 10^{-4}$, weight decay 10^{-4}) with cosine annealing to $\text{lr}_{\min} = 10^{-5}$, 300 epochs, batch size 256, mixed-precision, gradient clipping at norm 1.0, single seed (42), single GPU.

C NoisyMNIST: Gumbel-Sinkhorn Comparison

C.1 Method

We use the trained model's encoder and velocity network to extract a score matrix $S = \text{velocity}(\text{encoder}(\text{images})) \in \mathbb{R}^{N \times N}$, then apply Gumbel-Sinkhorn sampling:

$$\hat{X}^{(k)} = \text{Sinkhorn}\left(\frac{S + G^{(k)}}{\tau},\ n_{\text{iters}}\right), \quad G_{ij}^{(k)} \sim \text{Gumbel}(0,1) \text{ i.i.d.}$$

Each $\hat{X}^{(k)}$ is rounded via the Hungarian algorithm. We use log-domain Sinkhorn ($n_{\text{iters}} = 20$) and sweep $\tau \in \{0.05, 0.1, 0.2, 0.5, 1.0, 2.0, 5.0\}$.

C.2 Why Gumbel-Sinkhorn Fails on NoisyMNIST

Gumbel-Sinkhorn achieves $\approx 0\%$ **clean accuracy and** 0% **coverage at all temperatures and all** K (Table 1). Two structural causes combine to produce this failure.

Cause 1: velocity $\neq$ assignment score. The bilinear output $S[i,j] = \langle h_i, r_j \rangle / \sqrt{d}$ of the velocity network is trained via the CFM loss to produce the correct *direction of movement* in the Birkhoff polytope — not an assignment log-probability. Applying Gumbel noise to this velocity score and running Sinkhorn normalisation yields a doubly-stochastic matrix whose mass is spread nearly uniformly, because S was not calibrated to peak at the correct permutation entries. Hungarian rounding of a near-uniform matrix is dominated by small numerical perturbations, giving effectively random permutations ($\approx 0.1\%$ accuracy).

Cause 2: fixed velocity cannot resolve bimodal ambiguity. In the CFM model, diversity across K trajectories arises from different noisy starts X_0: the velocity $v = T(S)$ is the same for all trajectories, but distinct starting points $X_0 + v$ land in different regions of DS_N and round to different permutations. Gumbel-Sinkhorn has no equivalent geometry — it adds noise directly to the score rather than to the starting point of a flow — and with a miscalibrated score S it cannot recover either valid permutation.

Degenerate calibration. Since no valid permutation is ever found, $\hat{f}_a = 0$ for all samples. The blend weight $\alpha \sim \mathrm{Beta}(2, 2)$ has mean 0.5, so calibration error $= |\hat{f}_a - \alpha| = \alpha \approx 0.5$, giving the observed ≈ 0.504.

D SLAP: Experimental Details

D.1 Dataset Construction

Instances are generated synthetically with $C = C^\top$ maintained at every step. A noise base is formed as $C \leftarrow (\tilde{C} + \tilde{C}^\top)/2$ with $\tilde{C}_{ij} \sim \mathcal{N}(0,\, 0.25^2)$; all structured writes are applied symmetrically to both $C[r, c]$ and $C[c, r]$.

Clean (unimodal) instances. Each row k receives a distinct large negative bonus drawn from $\mathrm{Unif}(1.5,\, 2.5)$ at its target column $P_a[k]$, written symmetrically. Distinct bonuses ensure no pair of rows can be swapped without strictly increasing the cost, giving a unique labeled optimum confirmed by the Hungarian algorithm.

Bimodal instances. Starting from a random base permutation P_a, two rows i, j are selected and P_b is formed by swapping their assignments. Non-swap rows receive distinct bonuses as in the clean case. The four critical entries $\{(i, P_a[i]),\, (j, P_a[j]),\, (i, P_b[i]),\, (j, P_b[j])\}$ and their transposes are set *last* to a common tied value

$$c_{\mathrm{tie}} \sim -\mathrm{BonusHi} - \mathrm{Unif}(0.5,\, 1.5),$$

chosen strictly below -2.5, guaranteeing $\mathrm{cost}(P_a) = \mathrm{cost}(P_b)$ exactly. Both modes are verified by the Hungarian algorithm; constructions that fail fall back to clean instances.

Dataset splits. The training set contains 100,000 instances with a 50% bimodal target; 49,078 of the 50,000 bimodal attempts fail the strict optimality check and fall back to clean, giving an effective bimodal fraction of $\approx 1\%$. Separate test sets of 2,000 clean and 2,000 bimodal instances are drawn from an independent random stream.

D.2 Model and Optimization

Architecture. Each row $C[i, :] \in \mathbb{R}^n$ is projected to $d_{\mathrm{model}} = 128$, augmented with a learnable row-position embedding, and processed by a 2-layer Transformer (4 heads, FFN multiplier 4, dropout 0.1, GELU, pre-norm), yielding per-row contextual embeddings $h \in \mathbb{R}^{n \times d_{\mathrm{model}}}$. The velocity network prepends a state token—the flattened current position $X_t \in \mathbb{R}^{n^2}$ linearly projected to d_{model}—to the n cost embeddings and processes the resulting $(n+1)$ tokens with a 4-layer Transformer of the same configuration. A bilinear head produces $v \in \mathbb{R}^{n \times n}$, projected onto the doubly-stochastic tangent space (zero row/column-sum directions) before each Euler step.

At inference K independent trajectories are initialised as

$$X_0 = \mathcal{C}\big(\tfrac{1}{n}\mathbf{1}\mathbf{1}^\top + \sigma_0\, \varepsilon\big), \qquad \sigma_0 = 0.5,$$

where $\mathcal{C}$ is the tangent-space projection and ε is a doubly-centred matrix with unit Frobenius norm. After 20 Euler steps each trajectory is rounded to a hard permutation via the Hungarian algorithm.

Training. AdamW ($\mathrm{lr} = 3 \times 10^{-4}$, weight decay 10^{-4}) with cosine annealing to $\mathrm{lr}_{\min} = 10^{-5}$, 300 epochs, batch size 256, mixed-precision, gradient clipping at norm 1.0, single seed (42), single GPU. The model has 1.25M parameters (encoder 402K, velocity network 848K) and trains in ≈36 minutes on one H100.

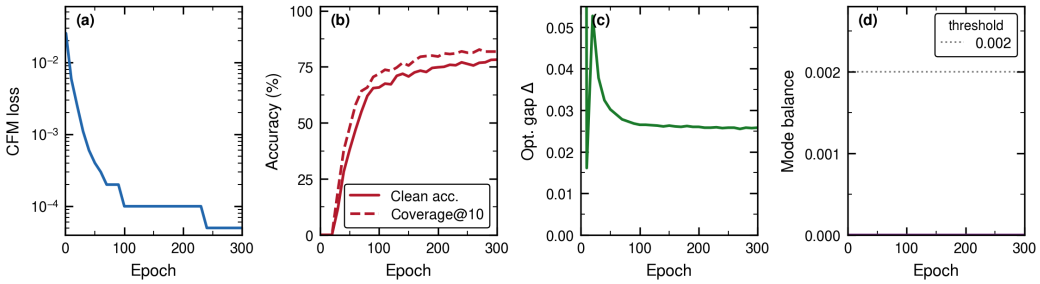

Figure 6: SLAP training dynamics ($N = 100$).

E SLAP: Gumbel-Sinkhorn Comparison

E.1 Method

Gumbel-Sinkhorn [Mena et al., 2018] draws K independent samples by adding iid Gumbel noise to the negated cost matrix and applying Sinkhorn normalisation:

$$\hat{X}^{(k)} = \mathrm{Sinkhorn}\left(\exp\left(\frac{-C+G^{(k)}}{\tau}\right),\ n_{\mathrm{iters}}\right), \quad G_{ij}^{(k)} \sim \mathrm{Gumbel}(0,1) \text{ i.i.d.}$$

Each $\hat{X}^{(k)}$ is rounded to a hard permutation via the Hungarian algorithm. We implement log-domain Sinkhorn for numerical stability (operating on $(-C+G)/\tau$ throughout and exponentiating only at the end). We sweep $\tau \in \{0.05, 0.1, 0.2, 0.5, 1.0, 2.0, 5.0\}$ with $n_{\mathrm{iters}} = 20$ and evaluate at $K \in \{5, \ldots, 100\}$.

E.2 Why Gumbel-Sinkhorn Fails on SLAP

Gumbel-Sinkhorn achieves **0% on all metrics at all temperatures and all** K (Table 2). Two structural causes combine to produce this failure.

Cause 1: cost-matrix symmetry removes the learning signal. Because $C = C^\top$, the score matrix $-C$ is also symmetric. For any labeled target permutation P_a, its matrix inverse P_a^{-1} satisfies

$$\mathrm{cost}(P_a^{-1}) = \sum_i C\big[i,\, P_a^{-1}[i]\big] = \sum_j C[P_a[j],\, j] = \sum_j C[j,\, P_a[j]] = \mathrm{cost}(P_a),$$

where the third equality uses $C = C^\top$. Hence every bonus entry $(k,\, P_a[k])$ in the cost matrix has an equally attractive symmetric partner $(P_a[k],\, k)$, and the score matrix $-C$ gives identical weight to P_a and P_a^{-1}. Gumbel-Sinkhorn has no access to the training distribution and therefore cannot prefer the labeled target over equally-cheap alternatives. Any of the multiple optimal permutations (including P_a^{-1}, P_b^{-1}, and other valid matchings on the bonus graph) may be returned; since the evaluation checks only for P_a and P_b, all other optimal assignments count as wrong.

Cause 2: incomplete Sinkhorn convergence inflates the cost gap. With $n_{\mathrm{iters}} = 20$, the Sinkhorn iteration has not converged for $n = 20$, leaving residual mass at non-bonus entries. The doubly-stochastic matrix is partially spread, and the Hungarian rounding produces a permutation that uses some non-bonus entries (near-zero cost positions), giving a cost ≈52% above the true optimum. This compounds the first failure: even if the method could in principle find P_a^{-1} (an equally optimal permutation), incomplete convergence means the sample is often not even optimal.

Degenerate mode balance. Gumbel-Sinkhorn reports mode balance $= 0.000$, which may appear to indicate perfect balance. It is in fact degenerate: both hit counts are zero (neither P_a nor P_b is ever recovered), so $|\mathrm{freq}(P_a) - \mathrm{freq}(P_b)| = |0 - 0| = 0$.

F Unbiasedness of PermFlow vs. Mode Collapse of Sinkhorn

This appendix formalizes the contrast claimed in the main text: PermFlow, in the population limit, places positive probability on every valid permutation mode, while Sinkhorn cannot place mass on more than one mode regardless of temperature or randomization at the score level.

F.1 Setup

Fix a finite set of valid target permutations $\{P_1, \ldots, P_M\} \subset \mathcal{B}$, and let μ_0 be a probability distribution on $\mathcal{B}$ representing the noisy initialization (e.g. $X_0 = \mathcal{C}(\frac{1}{n}\mathbf{1}\mathbf{1}^\top + \sigma_0\varepsilon)$ with $\varepsilon \sim \mathcal{N}(0, I)$). The nearest-target coupling assigns each initialization to the closest target in Frobenius norm:

$$P^\star(X_0) \;=\; \operatorname*{arg\,min}_{P \in \{P_1, \ldots, P_M\}} \|X_0 - P\|_F. \tag{21}$$

This partitions $\mathcal{B}$ (up to a measure-zero boundary) into the Voronoi cells

$$V_i \;=\; \{X \in \mathcal{B} : \|X - P_i\|_F < \|X - P_j\|_F \text{ for all } j \neq i\}, \qquad i = 1, \ldots, M. \tag{22}$$

F.2 Unbiasedness

Theorem 3 (Unbiasedness of PermFlow in the population limit)**.** *Suppose $\mu_0(V_i) > 0$ for every i, and let $v_\theta^\star$ minimize the population CFM objective*

$$L_{\mathrm{CFM}}(v) \;=\; \mathbb{E}_{t, X_0, P^\star}\Big[\, \big\|v(X_t, t) - (P^\star(X_0) - X_0)\big\|_F^2 \,\Big], \tag{23}$$

where $X_t = (1-t)X_0 + tP^\star(X_0)$. Let X_1 be the endpoint of the ODE $\dot{X}_t = v_\theta^\star(X_t, t)$ started at $X_0 \sim \mu_0$, and let $\hat{P} = \mathrm{Round}(X_1)$ be its Hungarian rounding. Then

$$\Pr[\hat{P} = P_i] \;=\; \mu_0(V_i) \;>\; 0 \qquad \textit{for every } i. \tag{24}$$

Proof. The conditional CFM objective is minimized pointwise by the constant conditional velocity along each straight-line interpolant:

$$v_\theta^\star(X_t, t) \;=\; \mathbb{E}\big[\, P^\star(X_0) - X_0 \;\big|\; X_t \,\big]. \tag{25}$$

For $X_0 \in V_i$, the conditional target is constant: $P^\star(X_0) = P_i$ almost surely, so along the straight line from X_0 to P_i the optimal velocity is exactly $P_i - X_0$. Integrating from $t = 0$ to $t = 1$ yields $X_1 = P_i$, which Hungarian rounding fixes as P_i. Hence $\hat{P} = P_i$ whenever $X_0 \in V_i$, and the claim follows from $\Pr[X_0 \in V_i] = \mu_0(V_i) > 0$. □

Corollary 4 (Mode coverage)**.** *Under the assumptions of Theorem 3, drawing K i.i.d. samples $X_0^{(1)}, \ldots, X_0^{(K)} \sim \mu_0$ and rounding their ODE endpoints yields a sample that covers every mode with probability tending to 1 as $K \to \infty$.*

F.3 Sinkhorn is structurally biased

Proposition 5 (Sinkhorn cannot represent multimodal distributions)**.** *Let $\mathcal{S}_\tau : \mathbb{R}^{n \times n} \to \mathcal{B}$ denote the entropy-regularized Sinkhorn operator at temperature $\tau > 0$, and let $R : \mathcal{B} \to \mathcal{P}_n$ be any rounding rule (e.g. Hungarian). For any score matrix S,*

$$R\big(\mathcal{S}_\tau(S)\big) \in \mathcal{P}_n \tag{26}$$

is a single permutation. In particular, for any distribution ν over score matrices, the induced distribution over rounded outputs satisfies

$$\Pr[\hat{P} = P_i] \in \{0, 1\} \tag{27}$$

whenever ν is concentrated on a single S. More generally, the support of the output distribution is at most a single permutation per score realization, so a deterministic input S can never produce mass on two distinct permutations.

Proof. $\mathcal{S}_\tau$ is the unique fixed point of alternating row and column normalization on $\exp(S/\tau)$ [Sinkhorn, 1964], hence a deterministic function of S. Composition with any deterministic rounding rule remains deterministic, so the output is a point mass for each fixed S. □

F.4 Discussion

Theorem 3 establishes unbiasedness for the *optimal* velocity field. The trained network v_θ approximates $v_\theta^\star$ but does not equal it, which is the source of the residual calibration error (≈ 0.18) reported in our experiments. This is a finite-sample training gap, not a structural limitation of the method. Proposition 5, in contrast, shows that no amount of training, tuning, or temperature selection can give Sinkhorn nontrivial mode coverage on a fixed input: the limitation is structural. Stochastic variants such as Gumbel-Sinkhorn inject noise at the score level and so escape the deterministic argument above, but as observed empirically in our experiments, their samples concentrate around a single soft assignment rather than partitioning mass across distinct permutation modes.